Available online at www.CivileJournal.org

Civil Engineering Journal

Vol. 5, No. 9, September, 2019

Failure Mode and Stability of Excavation Face on Shield Tunnel Undercrossing Existing Tunnel

Fei Xue [a*], Mengxi Zhang [a]

[a] *Department of Civil Engineering, Shanghai University, Shanghai200444, China.*

Received 14 June 2019; Accepted 22 August 2019

Abstract

The supporting pressure value of excavation face directly determines the stable state of excavation face, and its value will directly lead to instability of excavation face if the value is too small. When the shield is underneath the existing tunnel, special attention should be paid to the support pressure setting of the shield working face. When setting support pressure, the rigidity constraint of existing tunnel on surrounding soil should be fully considered. In this paper, we used ABAQUS software to analyse the failure mode of the soil around the existing tunnel due to the instability of the excavation surface caused by the small pressure setting of the excavation face, which is caused by the small pressure setting of the excavation face. By using the method of theoretical analysis, we optimized the prism in the traditional wedge model to chamfer platform with different opening angles to make it closer to the actual situation, and calculated the critical support pressure of shield tunnel face when it passes through the built tunnel. The research results can provide a reference for the effective value of support force of shield excavation face when the shield tunnel passes under the existing tunnel at a short distance.

Keywords: Shield Tunnel; Short-distance Construction; Support Pressure of Shield Face; Numerical Simulation; Wedge Model.

1. Introduction

In recent years, with the development of underground engineering, the construction of new tunnels crossing existing tunnels is increasing day by day, which is one of the unavoidable projects in the process of tunnel development. The instability of excavation will lead to cracking and leakage of existing tunnels, affect the normal use of tunnels, and even pose a serious threat to the safety of existing tunnel structures, surface traffic and surface buildings. How to minimize the impact of adjacent construction on the environment is the key to the adjacent construction of underground structures, which has attracted extensive attention from underground and geotechnical engineering circles [1-7].

Although the predecessors have done a lot of research on the construction of tunnel crossing and the stability of excavation face under various working conditions [8-10], there are still no research results on the stability of excavation face of new tunnel crossing existing tunnel working conditions. In practical engineering, unstable failure of excavation face, surface subsidence, cracking and leakage of existing tunnel caused by insufficient support pressure of excavation face are very concerned problems. Therefore, we focus on the stability of excavation face on shield tunnel undercrossing existing tunnel.

For the study of stability of excavation face, indoor and outdoor experiments, numerical simulation, theoretical analysis and field test are often used [11-13]. Miao (2015) analysed the soil damage form and distribution range of the shield tunnel excavation in sand environment, and on this basis, proposed the calculation of optimizing the minimum

* Corresponding author: fei_lin@126.com

http://dx.doi.org/10.28991/cej-2019-03091394

supporting force of the excavation face by the wedge model [14]. Xu (2012) used a three-dimensional wedge model based on limit equilibrium theory to study the stability of excavation surface of super-large diameter slurry shield [15]. Jancsecz (1994) and others used the principle of limit equilibrium to build a wedge model, and analyzed the ultimate support force of the excavation surface in the shield construction process and studied it. What's more, the ultimate support force of the excavation face in the shield construction is analysed and studied [16]. The collapse of the excavation face is used to simulate the failure mode of the excavation surface by the particle flow software. The traditional wedge model is optimized and optimized (HU, 2010) [17].

From all the above, it can be seen that the special form of short distance travelling has not been considered in the existing tunnels. The constitutive model of ABAQUS software is more suitable for geotechnical engineering. It can not only build models, generate grids and analyze them, but also analyze and calculate the pre-processing data generated by other drawing software directly. The numerical solutions are more realistic and suitable for the shield excavation analysis, and can provide theoretical guidance required for design of shield tunnelling. In view of the situation of shield tunnel crossing under existing tunnels, we used ABAQUS software to simulate the instability failure caused by too small support force on excavation face, and analyzed the failure shape. Then, we optimized the wedge model by theoretical analysis, and calculated the critical supporting pressure. Finally, we compared the values derived from wedge model with numerical simulation. Figure 1 is the flow chart of the research methodology.

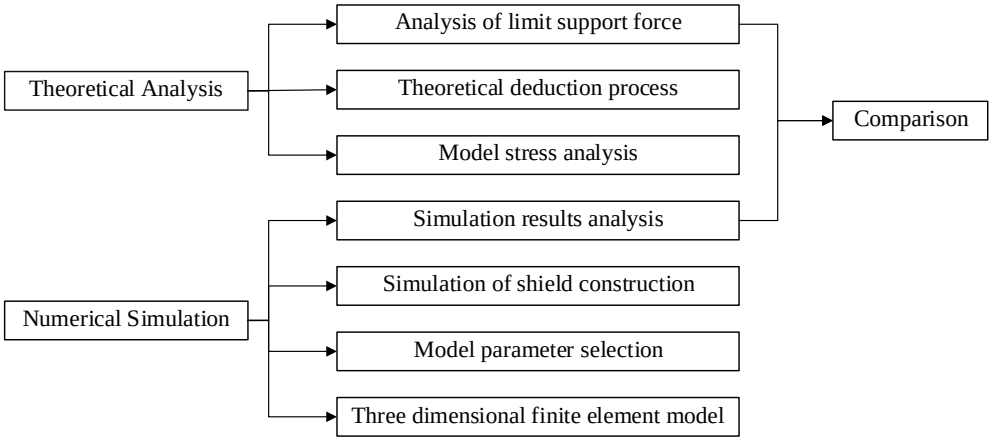

Figure 1. The flow chart of the research methodology

2. Numerical Simulation of Failure Mode of Excavation Face

2.1. Three Dimensional Finite Element Model

A three-dimensional model is established to simulate the instability of the excavation face caused by too small support pressure on the excavation face when the shield tunnels are close to the existing tunnels at different locations (H=1.5m, 3m, 4.5m). The size and meshing of the model are shown in Figure 2.The boundary condition of the model is assumed: the first is that all sides limit its normal displacement, the second is that the bottom is set to full constraint, and the third is the surface of the ground as the free plane, so that the change of the boundary condition will not have any effect on the vertical deformation of the model.

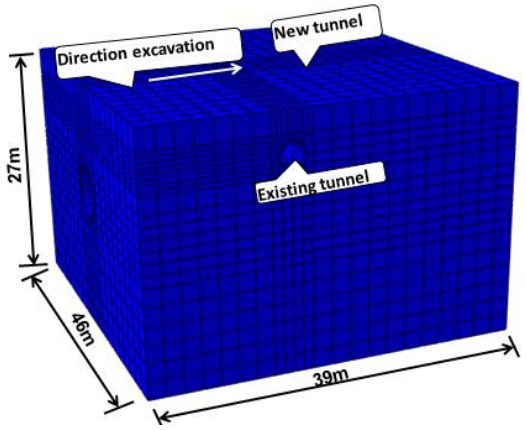

Figure 2. Three dimensional FEM model of shield crossing

2.2. Model Parameter Selection

The three dimensional hexahedron eight node solid element C3D8R is used in the soil and concrete segment, and the total number of solid elements in the model is 12305. Because the focus of this study is the stability of the excavation surface, in order to facilitate the calculation, the soil in the model is set as homogeneous soil. The constitutive model of the soil is Mohr-Coulomb model, and the physical and mechanical parameters of the model are shown in Table 1. The inside and outside diameters of the existing tunnels are 2.6m and 3M respectively, and the thickness of lining segments is 0.2m. The inside and outside diameters of the new tunnel are 5.2m and 6m respectively, and the thickness of lining segments is 0.4m. The concrete used for the lining of new and existing tunnel is C50, and according to the code, the elastic modulus of tunnel is 30GPa and Poisson's ratio is 0.2. Because the stability of excavation faces is mainly studied, the coupling effect between groundwater and soil is not considered.

Table 1. Physical and mechanical parameters of soils

parameter	Severe kN/m^3	Cohesive force kPa	Internal friction angle °	Modulus of elasticity MPa	Poisson ratio *v*
Value	17	4.5	10	20	0.35

2.3. Simulation of Shield Construction

When the dynamic process of shield tunneling is simulated, shield tunneling can be assumed to be discontinuous. In ABAQUS finite element software, the birth and death element function is used to simulate the excavation process, and the method of changing the material parameters of equipollent layer is used to realize the process of gap closure and synchronous grouting at the tail of shield. This paper focuses on the stability of the excavation face. Therefore, using one excavation to the designated location, at the same time, initial force is applied to support the excavation face, then the support force is released gradually until the excavation face is destroyed. Through the simulation, we found that the soil displacement perpendicular to the excavation direction is symmetrical distribution during shield tunneling. For example Figure 3, in order to improve the efficiency of the analysis, half of the model is selected. The finite element mesh is divided into Figure 4.

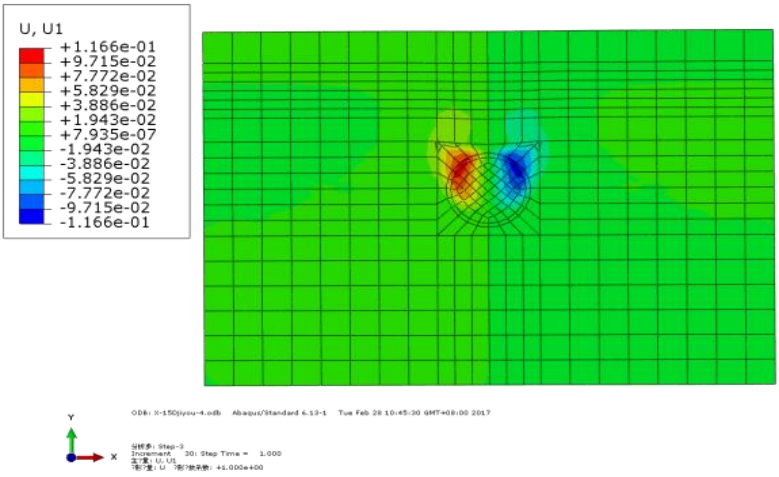

Figure 3. Horizontal displacement chart of soil in front of the shield (unit: m)

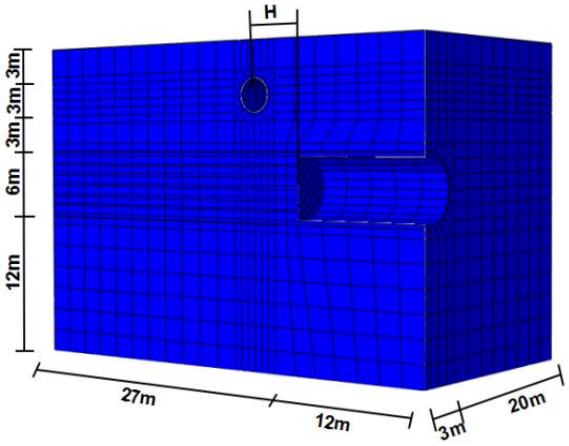

Figure 4. Mesh of finite element model (unit: m)

2.4. Simulation Results Analysis

When the support force reaches a critical state, the support force on the shield excavation face is gradually reduced at a slow speed. When the support force reaches the critical state, the node displacement in front of the excavation face will develop rapidly even if the change of the support force is very small, thus the soil will be greatly deformed, and the software can be terminated at this time. Figures 5, 6 and 7 are the failure modes of soil when the excavation face is 4.5m, 1.5m and 3M away from the existing tunnel.

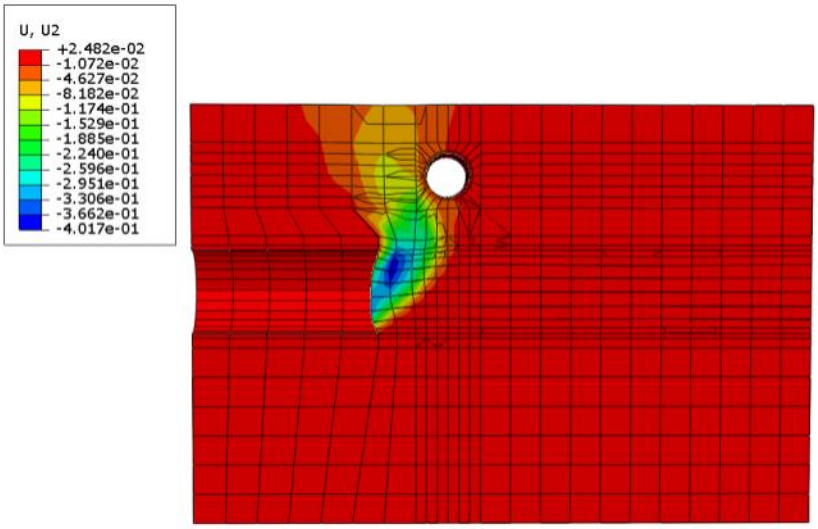

Figure 5. Soil failure modes at *H*=4.5m (unit: m)

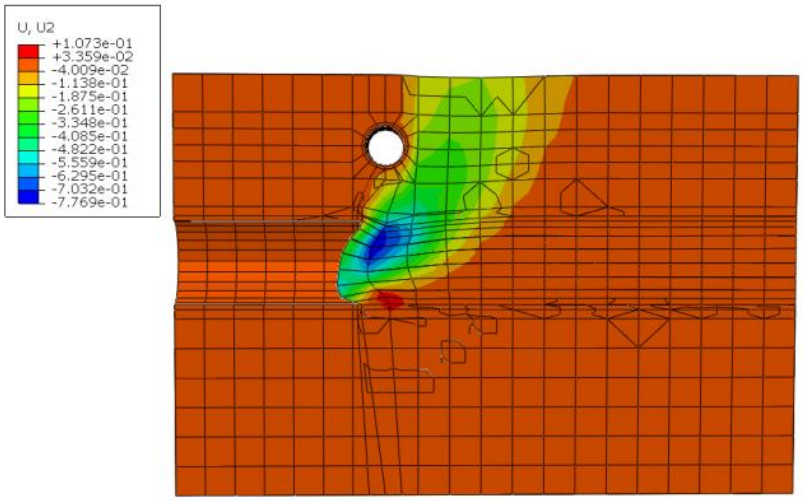

Figure 6. Soil failure modes at *H*=1.5m (unit: m)

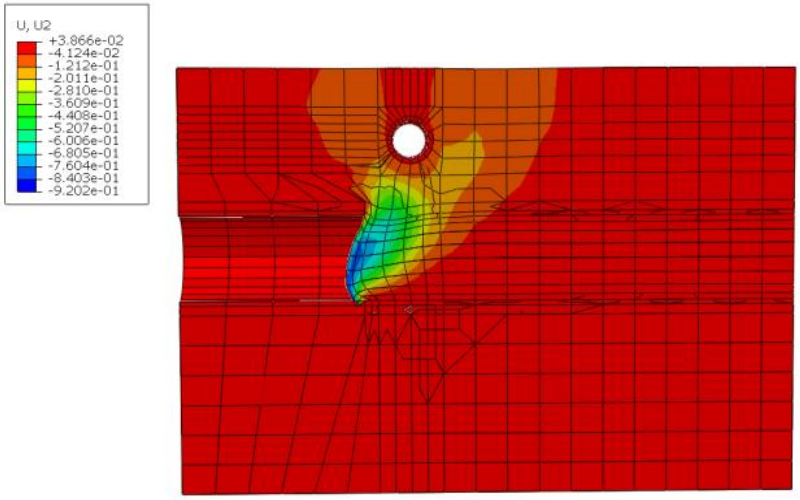

Figure 7. Soil failure modes at *H*=3m (unit: m)

The analysis of Figures 5 and 6 is not difficult to find that the sliding surface is asymmetrical along the direction of excavation two. As the stiffness of the tunnel is far greater than the stiffness of the surrounding soil, the damage area is restrained by the existing tunnel, so the opening angle of the sliding surface along the excavation direction is not equal, and the sliding angle of the sliding surface near the existing tunnel is relative to the sliding distance from the existing tunnel. The opening angle of the moving surface is small; Figure 7 is a special state in the process of excavation, that is, the existing tunnel is just in the central position of the damaged soil area, and the shape of the soil is destroyed symmetrically at this time, and the opening angle of the sliding surface on both sides of the tunnel is equal. In addition, from Figure 7, it is not difficult to find that the deformation of the soil at the top of the existing tunnel is very small, which may be because the stiffness of the existing tunnel is much larger than the stiffness of the surrounding soil, thus restraining the deformation of the soil above it.

By analyzing Figures 5 and 6, it is not difficult to find that the two sliding planes along the excavation direction are asymmetrical. Because the stiffness of the existing tunnel is much greater than that of the surrounding soil, the damage area is restrained by the existing tunnel, so the opening angles of the two sliding planes along the excavation direction are different. The opening angles of the sliding planes near the existing tunnel are smaller than those far away from the existing tunnel. Figure 7 is a special state in the excavation process, that is, the existing tunnel is located at the center of the damaged soil area, and the shape of the damaged soil is symmetrical distribution, and the opening angles of the sliding surfaces on both sides of the existing tunnel are equal. In addition, it is not difficult to find from Figure 7 that the deformation of the soil above the existing tunnel is very small, which may be due to the fact that the stiffness of the existing tunnel is much larger than that of the surrounding soil, thus restraining the deformation of the soil above it.

3. Theoretical Analysis of Three Dimensional Wedge Shape

The three-dimensional wedge model based on the limit equilibrium theory has been widely applied to the calculation of the limit support force of the excavation surface. The traditional wedge model consists of two parts of the wedge in front of the excavation surface and the prism above the wedge. Chen Renpeng (2013) optimized the traditional three-dimensional wedge model. The prism is changed into a chamfered platform with a certain angle of inclination, so that the damage area is closer to the actual uplift area of the soil [18]. Hu Xinyu and others assume that the opening angle of the sliding surface and the vertical direction of the shield in the three-dimensional wedge model is alpha, and the opening angle of the sliding surface and the vertical direction along the excavation direction is theta, which makes the damage area closer to the actual collapse area of the soil [17]. In this paper, the results of the numerical simulation show that the stiffness of the existing tunnel is much larger than that of the surrounding soil. When the supporting force is less than the critical value, the failure range of the soil will be restrained to a certain extent by the existing tunnel. Therefore, two sliding surface is asymmetrical along the direction of excavation face, the opening angle of sliding surface near existing tunnel is smaller than that of another sliding surface. Therefore, the three-dimensional wedge analysis model of excavation surface is optimized when existing tunnels exist in this paper, and optimizes the upper prism of the traditional wedge model into chamfered platform with different opening angles. The optimized three-dimensional wedge model is shown in Figure 8.

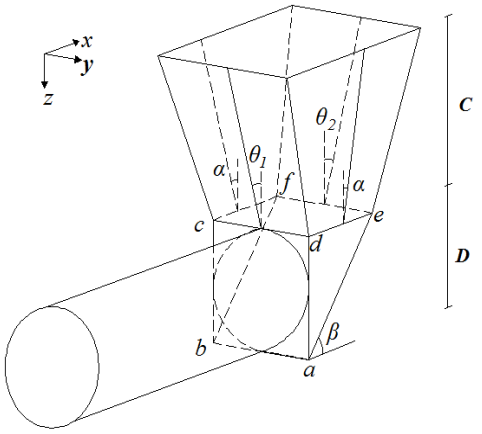

Figure 8. Optimized wedge mode

3.1. Model Stress Analysis

In the calculation process of the limit equilibrium method, it is assumed that the soil is uniform and isotropic, and the sliding of sliding surface in soil results in the destruction of soil, and the soil on the sliding surface is subject to the Mohr Coulomb failure criterion, and the shear strength formula of each element on each sliding surface in the soil can be expressed as $\tau = c + \sigma \tan \varphi$, and the internal structure of the lower wedge and the upper chamfered platform in the model is not deformed. According to the internal structure of inverted pyramid are not deformed, and meet the

conditions of static equilibrium.

Figure 9 is the stress analysis diagram of the optimized 3D wedge model. P is the ultimate supporting force of the excavation face in Figure 9(a). β is the dip angle of the lower wedge, G_1 is gravity, Q_2 is the resultant force on the inclined plane of the wedge, the Q_{3T} is the friction on the side, and the interaction force of the wedge and chamfered platform is Q_{1N}. In Figures 9(a) and 9(b), G_2 is for gravity. T_1 T_2 T_3 T_4 is as the friction on the bevel of chamfered platform, N_1 N_2 N_3 N_4 is as support force.

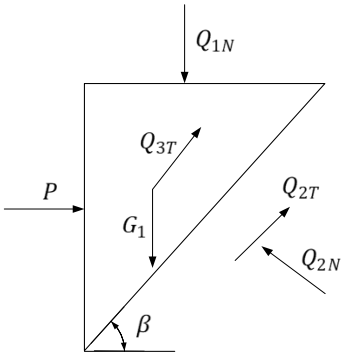

(a) Lower wedge

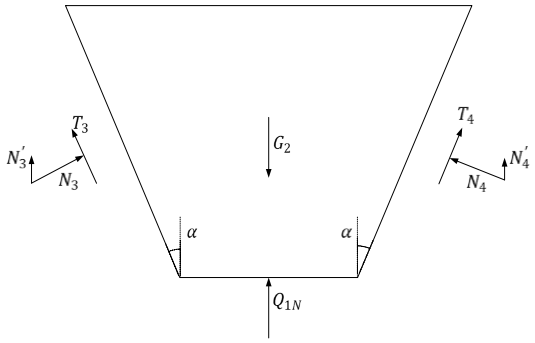

(b) Upper prism (perpendicular to excavation direction)

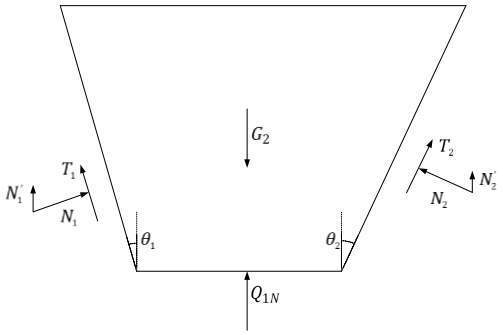

(c) Upper prism (parallel to excavation direction)

Figure 9. Stress diagram of optimized 3D wedge model

3.2. Theoretical Deduction Process

The first step takes the wedge as the object to analyze the force situation, and decomposes the force into the horizontal and vertical two directions, according to the zero resultant force of the two directions under the critical state, the corresponding equations are listed.

$$\sum F_Z = 0: \quad Q_{1N} + G_1 = \left(Q_{2T} + 2Q_{3T}\right)\sin\beta + Q_{2N}\cos\beta \tag{1}$$

$$\sum F_Y = 0: \quad P + \left(Q_{2T} + 2Q_{3T}\right)\cos\beta = Q_{2N}\sin\beta \tag{2}$$

$$Q_{2T} = \frac{\pi}{4} D^2 \cdot \frac{1}{\sin\beta} \cdot c_n + Q_{2N} \tan\varphi \tag{3}$$

By combining the above equations and eliminating Q_2, the formula for calculating the ultimate supporting force of excavation face can be obtained.

$$P = \frac{\sin\beta - \cos\beta\tan\varphi}{\cos\beta + \sin\beta\tan\varphi}\left[Q_{1N} + G_1 - \left(2Q_{3T} + \frac{\pi}{4} D^2 \cdot \frac{1}{\sin\beta} \cdot c_n \right) \sin\beta \right] - \left(2Q_{3T} + \frac{\pi}{4} D^2 \cdot \frac{1}{\sin\beta} \cdot c_n \right) \cos\beta \tag{4}$$

The self-weight of the wedge is as follows:

$$G_1 = \frac{\pi}{8} \gamma D^3 \cot\beta \tag{5}$$

The frictional force on the side sliding surface of the wedge:

$$Q_{3T} = \frac{\pi}{8} D^2 \cot\beta \cdot c_n + Q_{3N} \cdot \tan\varphi \tag{6}$$

Q_{3N} is the normal force acting on both sides of the wedge.

$$Q_{3N} = \frac{1}{2} K\gamma D^2 \cot\beta \left(C + \frac{1}{3} D \right) \tag{7}$$

K is the side pressure coefficient of soil. *K*=1-sinφ

The second step is to analyze the force acting on the prism, and the vertical equilibrium equation is as follows.

$$Q_{1N} + \left(T_1\cos\theta_1 + T_2\cos\theta_2 + T_3\cos\theta_3 + T_4\cos\theta_4 \right) + \left(N_1^{'} + N_2^{'} + N_3^{'} + N_4^{'} \right) = G_2 \tag{8}$$

In the form:

$$N_1^{'} = K\gamma C^2 \frac{\tan\theta_1}{\cos\theta_1} \left(\frac{\pi}{4} D + C \cdot \tan\alpha \right)$$

$$N_2^{'} = K\gamma C^2 \frac{\tan\theta_2}{\cos\theta_2} \left(\frac{\pi}{4} D + C \cdot \tan\alpha \right)$$

$$N_3^{'} = N_4^{'} = \frac{1}{2} K\gamma C^2 \frac{\tan\alpha}{\cos\alpha} \left(\begin{matrix} 2D\cot\beta + C\cdot\tan\theta_1 \\ +C\cdot\tan\theta_2 \end{matrix} \right)$$

$$T_1 = \left(\frac{\pi}{4} D + C \cdot \tan\alpha \right) \frac{C}{\cos\theta_1} \cdot c_n + \frac{N_1^{'}}{\sin\theta_1} \cdot \tan\varphi$$

$$T_2 = \left(\frac{\pi}{4} D + C \cdot \tan\alpha \right) \frac{C}{\cos\theta_2} \cdot c_n + \frac{N_2^{'}}{\sin\theta_2} \cdot \tan\varphi$$

$$T_3 = T_4 = \frac{1}{2} \left(\begin{matrix} 2D\cot\beta + \\ C\cdot\tan\theta_1 + C\cdot\tan\theta_2 \end{matrix} \right) \frac{C}{\cos\alpha} \cdot c_n + \frac{N_3^{'}}{\sin\theta_3} \cdot \tan\varphi$$

The Equations 5 to 8 was introduced into the Equation 4, and the ultimate supporting force of the excavation face was obtained.

$$P=\frac{\sin\beta-\cos\beta\tan\varphi}{\cos\beta+\sin\beta\tan\varphi}\left(A_1\cot\beta+A_2-A_3-A_5\right)$$

$$-A_4\cot\beta-\frac{\pi}{4}D^2\cot\beta\left(1+\cos\beta\right)\cdot c_n$$

Among:

$$A_1=\gamma D\left(\frac{\pi}{8}D^2+\frac{\pi}{4}CD+C^2\cdot\tan\alpha\right)$$

$$-2K\gamma C^2D\left(\frac{\tan\alpha}{\cos\alpha}+\frac{\tan\varphi}{\cos\alpha}\right)$$

$$A_2=\gamma C^2\left(\frac{2}{3}C\cdot\tan\alpha+\frac{\pi}{8}D\right)\left(\tan\theta_1+\tan\theta_2\right)$$

$$A_3=K\gamma C^2\left[\begin{array}{l}\left(\frac{\pi}{4}D+C\cdot\tan\alpha\right)\left(\frac{\tan\theta_1}{\cos\theta_1}+\frac{\tan\theta_2}{\cos\theta_2}+\frac{\tan\varphi}{\cos\theta_1}+\frac{\tan\varphi}{\cos\theta_2}\right)\\+C\left(\tan\theta_1+\tan\theta_2\right)\left(\frac{\tan\alpha}{\cos\alpha}+\frac{\tan\varphi}{\cos\alpha}\right)\end{array}\right]$$

$$A_4=K\gamma D^2\tan\varphi\left(C+\frac{1}{3}D\right)$$

$$A_5=\left[\begin{array}{l}D\cdot C\left(\frac{\pi}{2}+2\cot\beta\right)+\\C^2\left(2\tan\alpha+\tan\theta_1+\tan\theta_2\right)+\frac{\pi}{4}D^2\left(1+\cos\beta\right)\end{array}\right]c_n$$

3.3. Analysis of Limit Support Force by Limit Equilibrium Method

Through the optimized wedge analysis model, we obtained the relationship between ultimate supporting force and θ_1 and φ, as shown in Figures 10 and 11.

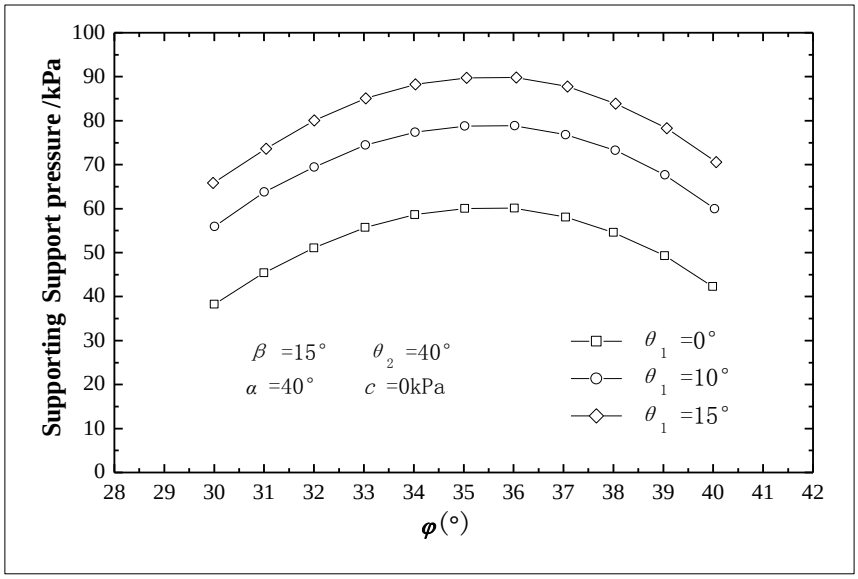

Figure 10. Variation of ultimate support stress with φ under different θ_1 conditions (c_n =0)

From Figure 10, we can see that the law of support pressure on excavation face varying with internal friction angle in sandy soil layer, it can be seen that when the internal friction angle is the same, the support pressure of the excavation face increases with the increase of θ_1. At the same time, when the internal friction angle φ increases, the pressure on

excavation face increases first and then decreases gradually like parabola. This is because the shield tunneling in the sandy soil will produce a significant soil arch effect, and the soil above the shield excavation face is constrained by the stiffness of the existing tunnel. In the figure, when the internal friction angle increases, the soil arching effect is more and more obvious, this is reflected in the gradual decrease of the critical support pressure on the excavation face.

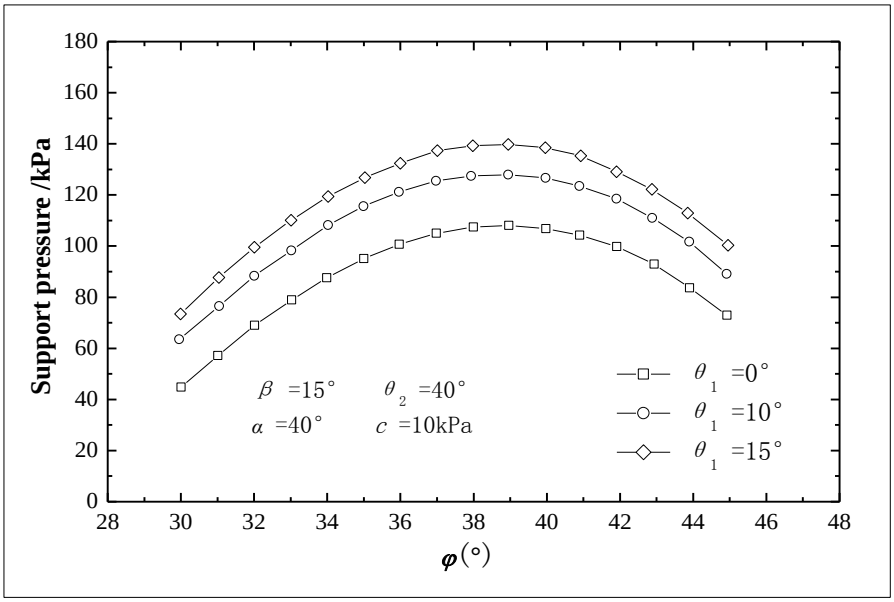

Figure 11. Variation of ultimate support stress with φ under different θ_1 conditions (c_n =10)

From Figure 11, we can see that the law of support pressure on excavation face varying with internal friction angle in viscous soil layer, and we also found that under the same internal friction angle, the pressure of the excavation face increases with the increase of θ_1. the law of support pressure on excavation face varying with internal friction angle φ, which is similar to that in the sandy soil layer. The main difference is that under the same parameter conditions, when the shield tunneling in the clay layer, the support pressure of excavation face is slightly higher than that in sandy soil, which is due to the weak soil arch effect in the viscous soil layer, and the support pressure for the stability of the excavation surface is slightly larger.

We calculated the numerical simulation scheme by the wedge model optimized in this paper, and compared the calculated results with the results calculated by the numerical simulation method in this paper. As shown in the data from Table 2, the results obtained by numerical simulation are slightly larger than those calculated by the optimized wedge model. This is probably due to the larger value predicted by numerical simulation when the plane strain is assumed. By comparing the optimized wedge model with the numerical simulation data, it is found that the two errors are within the allowable range. Therefore, it is also proved that the wedge-shaped analysis model after the optimization is reasonable and effective.

Table 2. Comparison between optimized wedge model and numerical simulation

Analysis method	φ		
	30	**35**	**40**
Optimized wedge model	41.4	75.9	71.4
Numerical calculation in this paper	42.2	77.1	72.6

4. Conclusions

In this paper, aiming at the failure problem of excavation face caused by too small support pressure when shield tunnels pass under existing tunnels at short distance, we revealed the failure mode by numerical simulation, and optimized the wedge model. Then, we deduced the analytical solution of critical support pressure by theoretical method. Finally, we carried out the theoretical analysis and compared the results with those obtained by numerical simulation. The conclusions are as follows:

- The numerical simulation results show that the stiffness of the existing tunnel is much larger than that of the surrounding soil. When the supporting force is less than the critical value, the failure range of the soil will be restrained to a certain extent by the existing tunnel. Therefore, the two sliding surfaces are asymmetric along the excavation direction, and the opening angle of the sliding surface near the existing tunnel is smaller than that of

the other sliding surface.

- No matter in sandy soil or clayey soil, when the angle of internal friction is the same, the supporting pressure will also increase with the increase of the friction angle. At the same time, because of the soil arch effect produced by the shield tunneling and the stiffness constraints of the tunnel on the top of the shield, the pressure of the excavation face increases first and then decreases like parabola with the increase of the internal friction angle.
- Under the same parameter conditions, when the shield tunneling in the clay layer, the support pressure of excavation face is slightly higher than that in sandy soil, which is due to the weak soil arch effect in the viscous soil layer, and the support pressure for the stability of the excavation surface is slightly larger.
- The results of numerical simulation are slightly larger than those of the wedge model optimized in this paper, and the rationality and validity of the wedge analysis model optimized in this paper are verified.

5. Funding and Acknowledgments

This work is supported by the National Natural Science Foundation of China (no. 41172238). China Railway 20 Bureau Group Co., Ltd., has also given a lot of practice guidance in the study of the paper.

6. Conflicts of Interest

The authors declare no conflict of interest.

7. References

[1] Ma J., Sun S. Z., Rui H. T., et al. “Review on China’s Traffic Engineering Research Progress: 2016.” China Journal of Highway and Transport (June 2016):1-161. doi:10.19721/j.cnki.1001-7372.2016.06.001.

[2] Li L., Zhang M. X., Wu H. M., et al. “Influence of short-distance multi-line overlapped shield tunneling on deformation of existing tunnels.” Chinese Journal of Geotechnical Engineering (June 2014): 1036-1043. doi:10.11779/CJGE201406007.

[3] Xiao X., Zhang M. X., Wu H. M., et al. “Numerical Simulation Analysis on Ground Settlements Caused by Multi-line Shield Tunnel.” Journal of Underground Space and Engineering (July 2011): 884-889. doi:10.3969/j.issn.1673-0836.2011.05.011.

[4] Yu N., Zhu H. H. “Analysis of earth deformation caused by shield tunnel construction and 3D-FEM simulation.” Rock and Earth Mechanics (August 2002): 1330-1334. doi:10.3969/j.issn.1000-7598. 2004.08.034.

[5] Chapman, D N, S K Ahn, and D VL Hunt. “Investigating Ground Movements Caused by the Construction of Multiple Tunnels in Soft Ground Using Laboratory Model Tests.” Canadian Geotechnical Journal 44, no. 6 (June 2007): 631–643. doi:10.1139/t07-018.

[6] Addenbrooke, T. I., and D. M. Potts. "Twin tunnel interaction: surface and subsurface effects." International Journal of Geomechanics 1, no. 2 (2001): 249-271. doi:10.1061/(ASCE)1532-3641(2001)1:2(249).

[7] Hefny A. M., Chua H. C., Zhao J. “Parametric Studies on the Interaction between Existing and New Bored Tunnels.” Tunnelling and Underground Space Technology 19, no. 4–5 (July 2004): 471. doi:10.1016/j.tust.2004.02.074.

[8] Zhang, Z.X., X.Y. Hu, and Kieffer D. Scott. “A Discrete Numerical Approach for Modeling Face Stability in Slurry Shield Tunnelling in Soft Soils.” Computers and Geotechnics 38, no. 1 (January 2011): 94–104. doi:10.1016/j.compgeo.2010.10.011.

[9] Xu Q. W., Tang Z. H., Zhu H. H., Wang G. F. “Limit support pressure at excavation face of shield tunnels.” Chinese Journal of Geotechnical Engineering (July 2017): 1234-1240. doi:10.11779/CJGE201707009.

[10] Sun X. H., Miao L. C., Lin H. S. “Arching effect of soil ahead of working face in shield tunnel in sand with various depths.” Rock and Soil Mechanics (October 2017): 2980-2988. doi:10.16285/j.rsm.2017.10.027.

[11] Wu J., Liao S. M., Wang K. “Experimental study on active failure modes of slurry shield-driven tunnel faces in sand.” Journal of Geomechanics (June 2018): 148-155. doi:10.12090/j.issn.1006-6616.2018.24.06.092.

[12] Liu H. N., Zhang Y. F., Liu H. D., Zhou J. J. “Experimental study on active failure modes of slurryshield-driven tunnel faces in sand.” Chinese Journal of Rock Mechanics and Engineering (March 2019): 572-581. doi:10.13722/j.cnki.jrme.2018.0920.

[13] Huang M. S., Li S., Yu J., Jorgin Q. W. T. “Continuous field based upper bound analysis for three-dimensional tunnel face stability in undrained clay.” Computers and Geotechnics (February 2018): 207-213. doi:10.1016/j.compgeo.2018.09.014.

[14] Miao L. C., Wang Z. X., Shi W. B. “Theoretical and numerical simulations of face stability around shield tunnels in sand.” Journal of Geotechnical Engineering (January 2015): 98-104. doi:10.11779/CJGE201501011.

[15] Xu M., Zou W. H., Liu Y. “Face stability of large slurry shield-driven tunnel in sands.” China Civil Engineering Journal (March 2012): 174–181. doi:10.15951/j.tmgcxb.2012.03.010.

[16] Jancsecz S., Steiner W . "Face support for a large mix-shield in heterogeneous ground conditions." Tunneling'94 (1994): 531–550. doi:10.1007/978-1-4615-2646-9_32.

[17] Hu X. Y., Zhang Z. X. "Stability Analysis Model of Shield Tunnel Based on Actual Failure Mode of Excavation Face." Journal of Shanghai Jiaotong University (September 2013): 1469-1476. doi:10.16183/j.cnki.jsjtu.2013.09.026.

[18] Chen R. P., Qi L. Z., Tang L. J., Zhou B. S. "Study on passive failure ultimate supporting force of shield tunneling face in sandy soil layer." Chinese Journal of Rock Mechanics and Engineering (January 2013): 2877-2882. doi:10.3969/j.issn.1000-6915.2013.z1.039.